Supporting Information

Pandelia et al. 10.1073/pnas.1100610108

SI Text

SI Materials and Methods. ***Purification and growth.*** The hyperthermophilic bacterium *Aquifex aeolicus* was grown at 85 °C in two-liter bottles under a $CO_2/H_2/O_2$ atmosphere. Hydrogenase I was purified at room temperature under semianaerobic conditions in a 50 mM Tris-HCl buffer pH 7.0, in the presence of 5–10% glycerol and 0.01% n-dodecyl-β-D-maltoside (DDM) as previously described (1). The enzyme used for Mössbauer measurements was obtained by isotope enriched growth of the bacterium with ^{57}Fe (metallic ^{57}Fe (∼95%) was purchased from Chemotrade, Düsseldorf, Germany). For this experiment the bacterium was grown at 85 °C in two-liter bottles under a $CO_2/H_2/O_2$ atmosphere in a media containing metal free water (GPR rectapur®, VWR) and all the others products were Fe free as much as possible. ^{57}Fe was first dissolved in concentrated HCl 37% and the media was supplemented by ^{57}Fe at 2 mg/l. Hase I was further purified as described for the nonlabeled case.

EPR spectroscopy. X-Band measurements were carried out using a continuous wave (cw) X-band Bruker ESP 300E instrument (9.4 GHz, TE_{012} resonator) equipped with a helium flow cryostat (Oxford Instruments, ESR910) and an ITC 503 temperature controller. cw S-band (2–4 GHz, loop gap resonator) and cw Q-Band (34 GHz, TE_{011} resonator) measurements were carried out using a Bruker ESP-300 spectrometer equipped with an Oxford Instruments helium flow cryostat. Pulse Q-Band experiments were carried out on a Bruker Elexsys E-500 FT EPR Q-band spectrometer with a helium flow cryostat and using a home-built resonator (2). cw and pulse W-band measurements were carried out in a Bruker Elexsys E-680 FT EPR W-band spectrometer with a helium flow cryostat and a variable-temperature TeraFlex Bruker resonator. Spin quantitations were carried out by using copper perchlorate as a standard under nonsaturating conditions (10 mM $CuSO_4$, 2 mM $NaClO_4$, 10 mM HCl).

Mössbauer spectroscopy. Mössbauer spectra were recorded on an alternating constant acceleration spectrometer. The minimum experimental line width was 0.24 mms^{-1} (full-width at half maximum). The sample temperature was maintained constant either in an Oxford Variox or an Oxford Mössbauer-Spectromag cryostat. The latter is a split-pair conducting magnet system for applying fields of up to 8 Tesla (T) to the samples that can be kept at temperatures in the range 1.5–250 K. The field at the sample is perpendicular to the γ beam. All isomer shifts are quoted relative to iron metal at 300 K.

Determination of redox potentials. Redox potentials were determined by cw EPR potentiometric titrations. The titration cell used is similar to the one described by Dutton (3). The error in the determination of the oxidation-reduction potentials is ±20 mV. The protein solution was kept under anaerobic conditions during the titration by flushing with hydrated argon gas, which was prior passed through an Oxisorb cartridge to remove residual traces of oxygen. The titration was carried out by adjusting the potential with substoichiometric amounts of solutions of sodium dithionite ($Na_2S_2O_4$) and potassium ferricyanide ($K_3[Fe(CN)_6]$). The temperature was maintained at 15 °C by cold water passing through the glassy body of the cell in a closed external circuit with a thermostat (LAUDA). The potentials were measured with a pH/redox meter (GPHR 1400, Greisinger) using a combination Pt/Ag/AgCl micro-electrode (3M KCl, Mettler Toledo) and are quoted relative to the normal standard hydrogen electrode. The electrode was calibrated with a saturated quinhydrone solution at pH 7.4 (1M Hepes buffer) based on the formula:

$$E = E_{\mathrm{st.qh}} - 0.1984(273.16 + T)\mathrm{pH}, \qquad \textbf{[S1]}$$

where $E_{\mathrm{st.qh}}$ is the measured potential of the saturated quinhydrone solution in mV and T the temperature in K. For the titration at pH 7.4 the buffering solution was 50 mM Hepes-NaOH and the following redox mediators were present at a final concentration of 100 μM, with the exception of phenazine methosulfate which was in a final concentration of 50 μM: 1,2-naphthoquinone (+145 mV), phenazine methosulfate (+90 mV), phenazine ethosulfate (+55 mV), methylene blue (+11 mV), indigo tetrasulfonate (−46 mV), 2- hydroxyl-1,4 naphthoquinone (−137 mV), anthraquinone-1,5-disulfonate (−170 mV), phenosafranine (−252 mV), safranine T (−290 mV), and benzyl viologen (−345 mV). Five percent of glycerol was added to the final redox solution to assist in dissolving of the redox mediators. For the pH dependent redox titrations buffering solutions of 100 mM MES-NaOH (pH 6.4) and 100 mM Tricine-NaOH (pH 8.3) were used. A modified mediator mixture was used consisting of: 1, 2-naphthoquinone-4-sulfonic acid, phenazine methosulfate, phenazine ethosulfate, methylene blue, vitamin K3, 2,3-dihydroxy-5-methyl-benzoquinone, 2-hydroxyl-1,4 naphthoquinone, anthraquinone-1,5-disulfonate, phenosafranine, safranine T, and benzyl viologen. The dependence of the reduction potentials of these electron reagents are described elsewhere (4). The forward titration (towards negative potentials) was carried out in approximately 60 mV steps while the backward titration (towards positive potentials) was performed in approximately 60 mV steps: as a result an EPR spectrum was taken every 30 mV. In this manner the reversibility of the process involved was controlled. Three hundred μL samples of 12 μM protein concentration were loaded in calibrated quartz EPR X-band tubes under a stream of argon gas and rapidly frozen in a cold liquid ethanol-nitrogen mixture.

Determination of pKa. The *pKa* values were determined using the Henderson-Hasselbalch relation (5):

$$E_m = E_m(\mathrm{lowpH}) + \frac{R \cdot T}{n \cdot F} \log\left[\frac{1 + 10^{(\mathrm{pKred\text{-}pH})}}{1 + 10^{(\mathrm{pKox\text{-}pH})}}\right], \qquad \textbf{[S2]}$$

where E_m are the experimentally obtained midpoint potentials, $E_m(\mathrm{lowpH})$ is the first formal midpoint potential for the protonation of the related amino acid, R the universal gas constant (8.3145 $JK^{-1}\,mol^{-1}$), F the Faraday constant (96,485 $C\,mol^{-1}$), n number of electrons, and T temperature (K).

Oxidation with porphyrexide ($C_5H_9N_4$). The porphyrexide (4-amino-2 imino-5,5-dimethyl-2,5-dihydro-1*H*-imidazole-1-oxyl) was synthesized in-house as described in (6). The purity of the compound was confirmed by IR spectroscopy and its midpoint potential was determined to be $E_m = +698$ mV in H_2O by cyclic voltammetry, which is very close to that reported elsewhere (7). The porphyrexide solution was freshly prepared in pure water on ice as it was found that it reacts with the Hepes/Tris buffers (most likely can oxidize them). A ten times excess of porphyrexide was shown to be adequate to superoxidize the hydrogenase sample from *A. aeolicus* ([3Fe4S] uncoupled signal was of the order of 5% or less), because part of it reacted most likely with the buffer itself (aerobic addition, total reaction time 10 min).

EPR spectra simulation. The full spin Hamiltonian for an exchange-coupled two-spin system can be written as (8):

$$H = -2J\vec{S}_1\vec{S}_2 + \vec{S}_1\mathbf{d}_{12}\vec{S}_2 + \sum_{i=1,2}\mu_B\vec{B}_0\mathbf{g}_i\vec{S}_i, \qquad \textbf{[S3]}$$

where the first term is the Heisenberg exchange. In this article, we consider only the isotropic part of the exchange coupling tensor J, because the anisotropic part is typically small and it is complicated to evaluate from EPR data. The second term in Eq. **S3** is the magnetic dipolar coupling. Dipolar coupling mainly depends on the distance between paramagnetic centers. Using the point-dipole approximation the tensor d_{12} can be expressed as:

$$\mathbf{d}_{12} = \frac{\mu_B^2}{r^3}\left(\mathbf{g}_1\mathbf{g}_3 - \frac{3(\mathbf{g}_1\vec{r})(\mathbf{g}_2\vec{r})}{r^2}\right), \qquad \textbf{[S4]}$$

where r is the distance vector between the two paramagnetic centers and g_1 and g_2 are the g-factors of the two ions (considered to be anisotropic). A more accurate description would require exact knowledge of the projection factors of the dipolar interaction between each Fe ion. The last term of 15Eq. **S3** contains the electronic Zeeman interaction.

1. Brugna-Guiral M, et al. (2003) [NiFe] hydrogenases from the hyperthermophilic bacterium *Aquifex aeolicus*: properties, function, and phylogenetics. *Extremophiles* 7:145–157.
2. Niklas J, et al. (2009) Electronic structure of the quinone radical anion A(1)(center dot-) of photosystem I Investigated by advanced pulse EPR and ENDOR techniques. *J Phys Chem B* 113:10367–10379.
3. Dutton PL (1978) Redox potentiometry: determination of midpoint potentials of oxidation-reduction components of biological electron-transfer systems. *Methods Enzymol* 54:411–435.
4. Prince RC, Linkletter SJG, Dutton PL (1981) The thermodynamic properties of some commonly used oxidation-reduction mediators, inhibitors and dyes, as determined by polarography. *Biochim Biophys Acta* 635:132–148.
5. DeLacey AL, Fernandez VM (1995) pH-dependent redox behavior of asymmetric viologens. *J Electroanal Chem* 399:163–167.
6. Tretyakov E, et al. (2006): Properties and structures of porphyrexides. *Russ Chem Bull* 55:457–463.
7. Kuhn R, Franke W (1935) The redox potential of porphyrexide and porphyrindine. *Berichte der Deutschen Chemischen Gesellschaft* 68:1528–1536.
8. Bencini A, Gatteschi D (1990) *Electron Paramagnetic Resonance of Exchange-Coupled Systems. Springer-Verlag New York, Inc.*

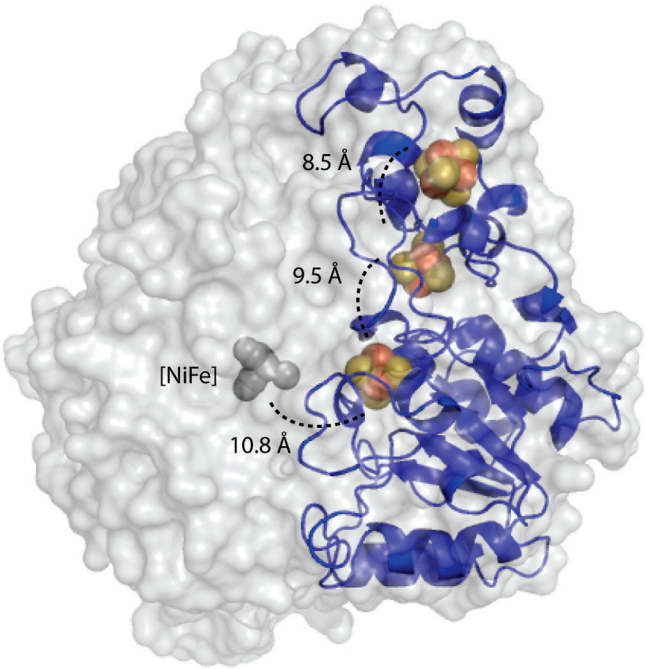

Fig. S1. Homology model of Hase I (shown as a blue ribbon) overlaid on the crystal structure of the standard [NiFe] hydrogenase from *D. vulgaris* MF (pdb entry 1WUJ) that is shown as surface in gray color and with the heteroatoms shown as spheres. This picture along with sequence alignment shows that the number of the iron-sulfur clusters and their topology is conserved between O_2-tolerant and O_2-sensitive enzymes. The three clusters based on their distance from the [NiFe] active site are termed as proximal (P), medial (M), and distal (D), respectively. In standard hydrogenases the proximal and the distal clusters are two low-potential [4Fe4S] cubanes and the medial cluster is a [3Fe4S] center. The only exception is the subclass of [NiFeSe] hydrogenases, where all three clusters are of the [4Fe4S] type (1). The closest metal-to-metal distances between the cofactors are given.

1 Garcin E, et al. (1999) The crystal structure of a reduced [NiFeSe] hydrogenase provides an image of the activated catalytic center. *Structure* 7:557–566.

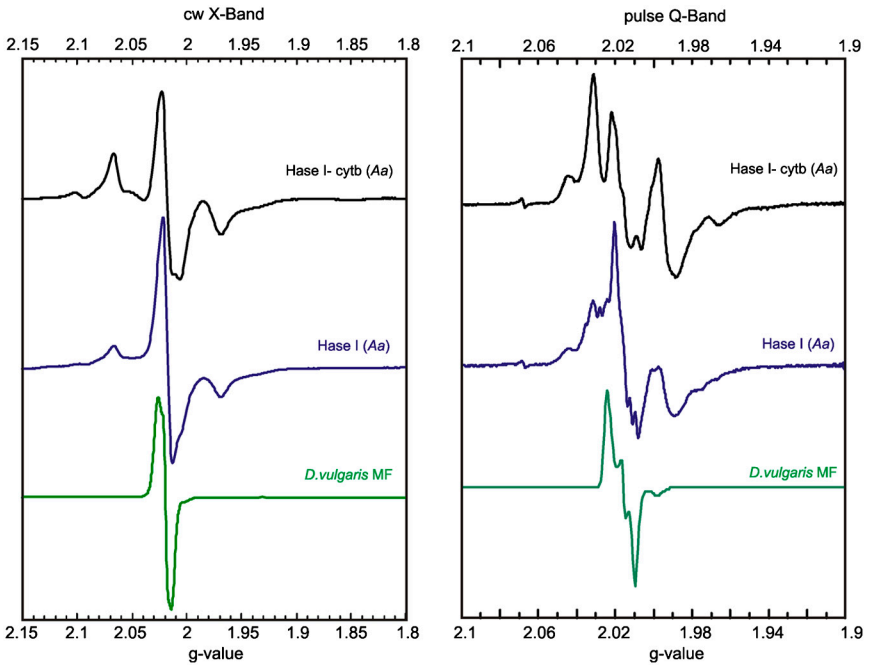

Fig. S2. (Left) cw EPR spectra at X-band and (right) pseudomodulated EPR spectra at Q-band frequency, recorded at 10 K, of different sample preparations of the *A. aeolicus* hydrogenase that was purified in the hetero-trimeric form as Hase I-*cyt*b complex and as a hetero-dimer (Hase I). The spectra of the as-isolated *D. vulgaris* Miyazaki F hydrogenase, which exhibit at low temperatures (<50 K) only a signal typical of an oxidized $[3Fe4S]^{1+}$ ($S = 1/2$) cluster with small g-anisotropy ($g_{iso} = 2.019$) (1), are included as a reference (green traces). (cw X-Band): temperature 10K, microwave frequency 9.47 GHz, modulation amplitude 0.5 mT (pulse Q-Band): temperature 10 K, microwave frequency 34 GHz, SRT 1 ms, pseudomodulation of the absorption spectra was performed with 1 mT modulation amplitude.

The microwave frequency dependence of the EPR spectra discards the possibility that the spectral features originate from *g*-anisotropy but shows that they are associated with a *J*-interaction between different centers. The yield of the coupled signals resulting from the interaction between the medial [3Fe4S] cluster and the HP center can vary between the various purifications. The uncoupled [3Fe4S] cluster contribution in the spectra of the Hase I-*cyt*b complex is of 20–25%. The same samples recorded at two different frequencies, provide insight as to which features in the Q-band can be assigned to the coupled system, showing that the "wings" of the spectra originate from the interaction between the two paramagnetic centers (Hase I). The occurrence of a less-spin coupled amount of centers in the heterodimer case is rather coincidental and not systematic. We believe that the different yields of the HP center in each case is a result of the different treatment of the samples and differences in the oxidative conditions experienced from the hydrogenase molecules during purification.

1 Brecht M (2001) Hochfeld- und Puls-EPR-Untersuchungen an den Kofaktoren von [NiFe]-Hydrogenasen: Beiträge zur Klärung des Mechanismusses der biologischen Wasserstoffspaltung,Technische Universität Berlin, Doctoral thesis.

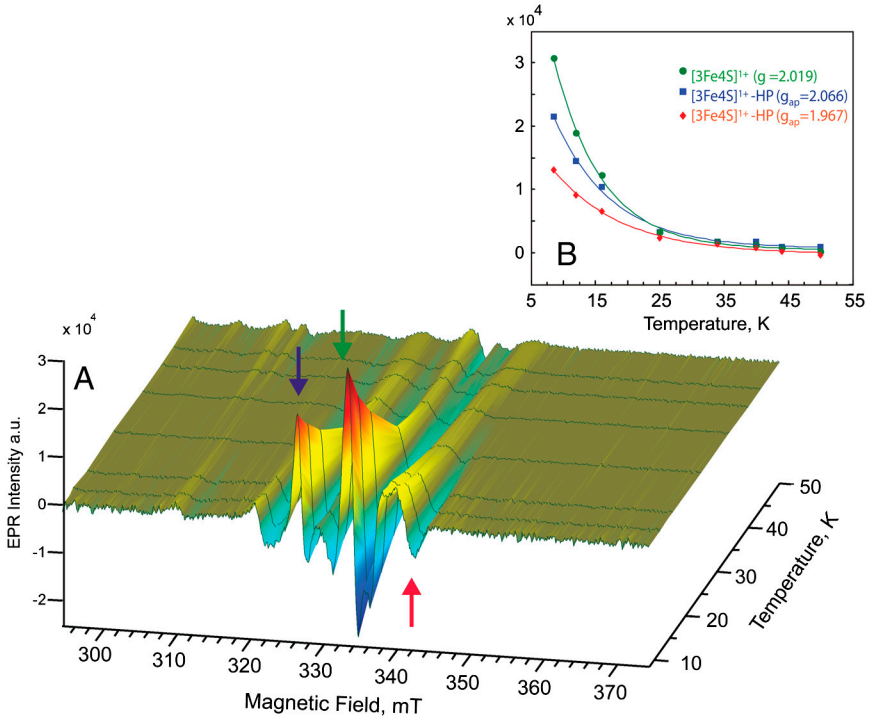

Fig. S3. (*A*) Three-dimensional representation of the cw X-Band EPR spectra corresponding to the complex iron-sulfur cluster signals of the as-isolated Hase I from *A. aeolicus* as a function of temperature (between 8 and 50 K). The inset (*B*) shows the temperature dependence of the most prominent features of the spectrum including the "uncoupled" $[3Fe4S]^{1+}$ signal and the "coupled" ($[3Fe4S]^{1+}$-HP) signal, indicated in the spectra by arrows in the respective colors. Experimental conditions: microwave frequency 9.436 GHz, modulation amplitude 0.3 mT, modulation frequency 100 kHz.

Above 50 K the signals of the clusters are broadened beyond detection. When increasing the temperature the signals are uniformly broadened and no individual spectra can be discerned, which agrees well with the result that these spectra correspond to magnetically coupled species. In addition, the spectra exhibit a relaxation behavior characteristic of iron-sulfur centers and do not indicate the presence of any slow relaxing "radical-like" species.

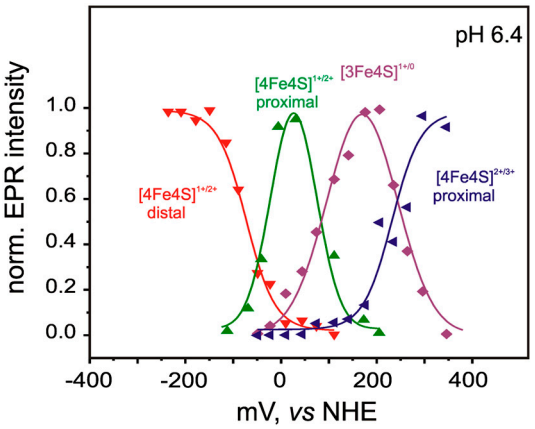

Fig. S4. EPR Redox titration of the iron-sulfur clusters of Hase I carried out at pH 6.4 as described in the Material and Methods section of the main text. The redox transitions have been assigned to the respective redox species, i.e., distal four-iron cluster (red triangles), the canonical transition of the proximal four-iron cluster (green triangles), the medial three-iron cluster (purple rhombuses) and the transition to the high potential form of the proximal four-iron cluster (blue tilted triangles), which are described in detail in the main text of the manuscript.

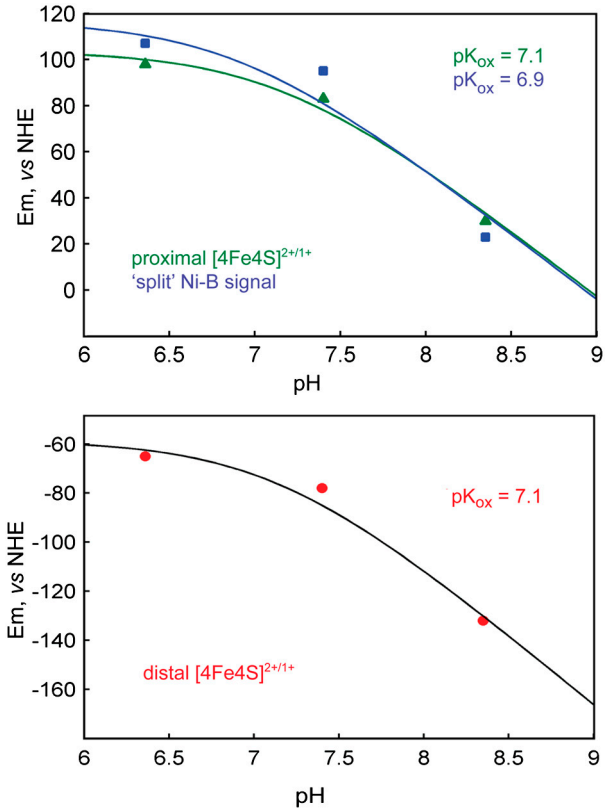

Fig. S5. pH dependence of the midpoint potentials of the proximal (top) and distal (bottom) iron-sulfur cluster of the $[4Fe4S]^{2+/1+}$ couples in Hase I. The appearance of the splitting patterns in the Ni-B EPR signals follow the same pH dependence with the reduction of the $[4Fe4S]^{2+/1+}$ couple showing that the latter is the proximal [4Fe4S] cluster. The reduction potentials of the iron-sulfur clusters are greatly affected by the ligands and the protein surrounding and it is likely that the presence of two additional cysteinyl residues in the protein fold of the proximal [4Fe4S] is to a large extent responsible for the very positive E_m (1).

1 Capozzi F, Ciurli S, Luchinat C (1998) Coordination sphere versus protein environment as determinants of electronic and functional properties of iron-sulfur proteins. *Metal Sites in Proteins and Models* 90:127–160.

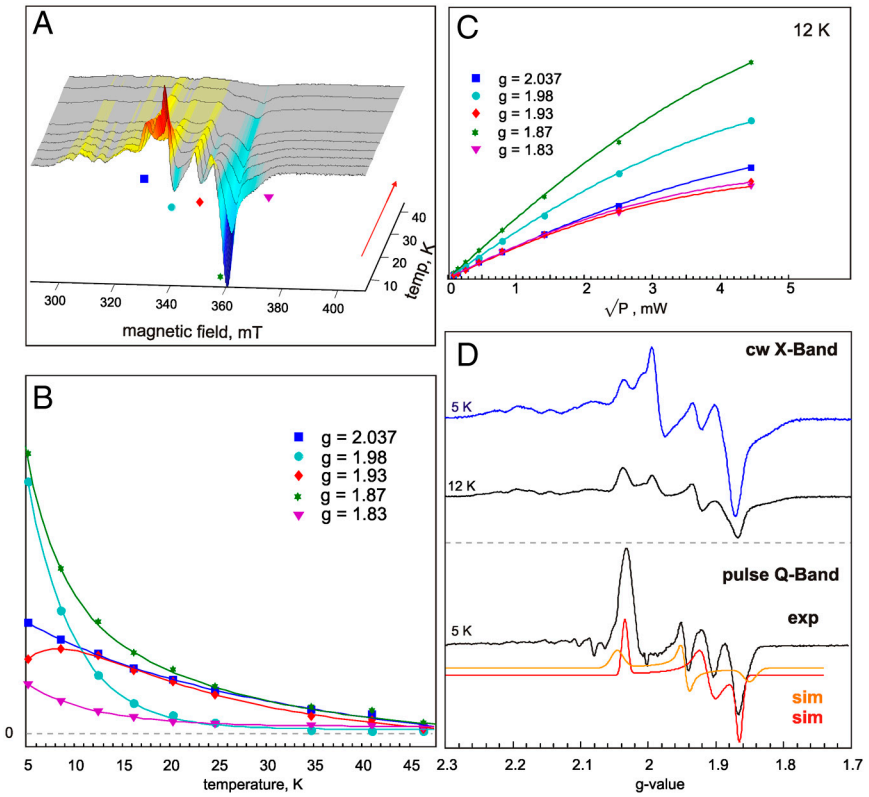

Fig. S6. cw X-band EPR spectra of the H_2-reduced Hase I. (*A*, *B*) three- and one- dimensional plots of the temperature dependence of the features corresponding to the H_2-reduced enzyme. The signals are well observed until 40 K after which they broaden and above 50 K they are hardly detectable. (*C*) Saturation curves of the signals of the reduced protein at 12 K. (*D*, top) cw X-band EPR spectra at 5 and 12 K. Note that the signals at 1.98 and 1.87 reduce most in intensity upon increasing the temperature. (*D*, bottom) 2-pulse-echo detected pseudomodulated Q-band EPR spectrum of the H_2-reduced enzyme at 5 K (spectrum was the same at 12 K). The signals at Q-band could be well simulated considering two uncoupled [4Fe4S] clusters with *g*-values (orange trace: $g_z = 2.044$, $g_y = 1.934$, $g_x = 1.854$, and red trace: $g_z = 2.033$, $g_y = 1.910$, and $g_x = 1.862$), which can be explained considering that the relaxation properties of the high spin reduced $[3Fe4S]^0$ ($S = 2$) are expected to be too fast to be detectable in these pulse measurements. Other experimental conditions: (X-Band) microwave frequency 9.438 GHz, microwave power 0.20 mW, modulation amplitude 0.7 mT, (pulse Q-Band): microwave frequency 34.04 GHz, SRT = 4 ms, $\pi/2 = 36$ ns. A broad feature at 2.086 is very easily saturated and it appears not to be associated with the signals of the reduced [FeS] clusters.

The fully reduced Hase I shows well defined and distinct signals in the [FeS] cluster region, in contrast to what has been previously reported for standard hydrogenases (1). This spectrum is proposed to be similar to standard hydrogenases and is the result of the coupled interaction of the two low-potential [4Fe] clusters ($S = 1/2$) and the high spin [3Fe] cluster ($S = 2$). Identical signals to the ones exhibited by Hase I are also observed for other O_2-tolerant enzymes (e.g., MBH from *R. eutropha*)(2).

1 Teixeira M, et al. (1989) Redox intermediates of *Desulfovibrio-gigas* [NiFe] hydrogenase generated under hydrogen—Mössbauer and EPR characterization of the metal centers. *J Biol Chem* 264:16435–16450.
2 Saggu M, et al. (2009) Spectroscopic insights into the oxygen-tolerant membrane-associated [NiFe] hydrogenase of *Ralstonia eutropha* H16. *J Biol Chem* 284:16264–16276.

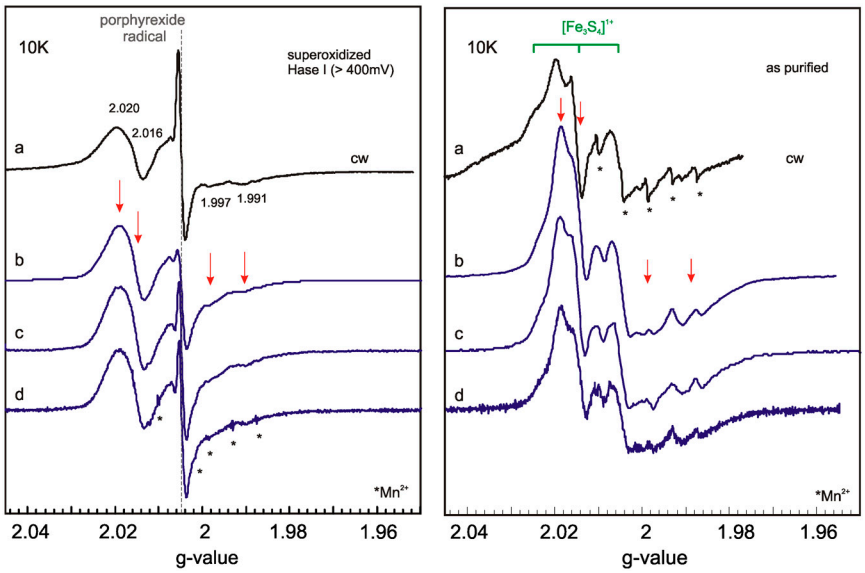

Fig. S7. Collection of cw (black trace) and 2-pulse echo detected (blue traces) pseudomodulated EPR spectra recorded at W-Band frequency (94 GHz) at 10 K. (Left) Spectra recorded for the superoxidized enzyme after addition of porphyrexide and (right) spectra recorded for the as-isolated enzyme. The signal of the porphyrexide radical (used as an oxidant) is indicated with the gray dashed line, whereas the contributions of the Mn^{2+} (originating from the resonator) are shown with asterisks. Red arrows mark the signals that correspond to the three-spin coupled system consisting of the HP species (superoxidized proximal [4Fe4S] cluster), the medial $[3Fe4S]^{1+}$ cluster and the [NiFe] site. Experimental conditions: SRT 0.5 ms, $\pi/2 = 24$ ns, pseudomodulation of the absorption spectra was performed with 1.0 mT modulation amplitude. The principal *g*-values of the medial [3Fe4S] cluster are given in Table S1 and are compared to the ones from *D. vulgaris* MF standard hydrogenase (1). Due to the manganese contributions in the spectra, all three principal components of the *g*-values of the medial cluster were resolved by measurements recorded in a home-built spectrometer operating at 244 GHz at 17 K and with a modulation amplitude of 0.3 mT.

1 Brecht M (2001) Hochfeld- und Puls-EPR-Untersuchungen an den Kofaktoren von [NiFe]-Hydrogenasen: Beiträge zur Klärung des Mechanismusses der biologischen Wasserstoffspaltung,Technische Universität Berlin, Doctoral thesis.

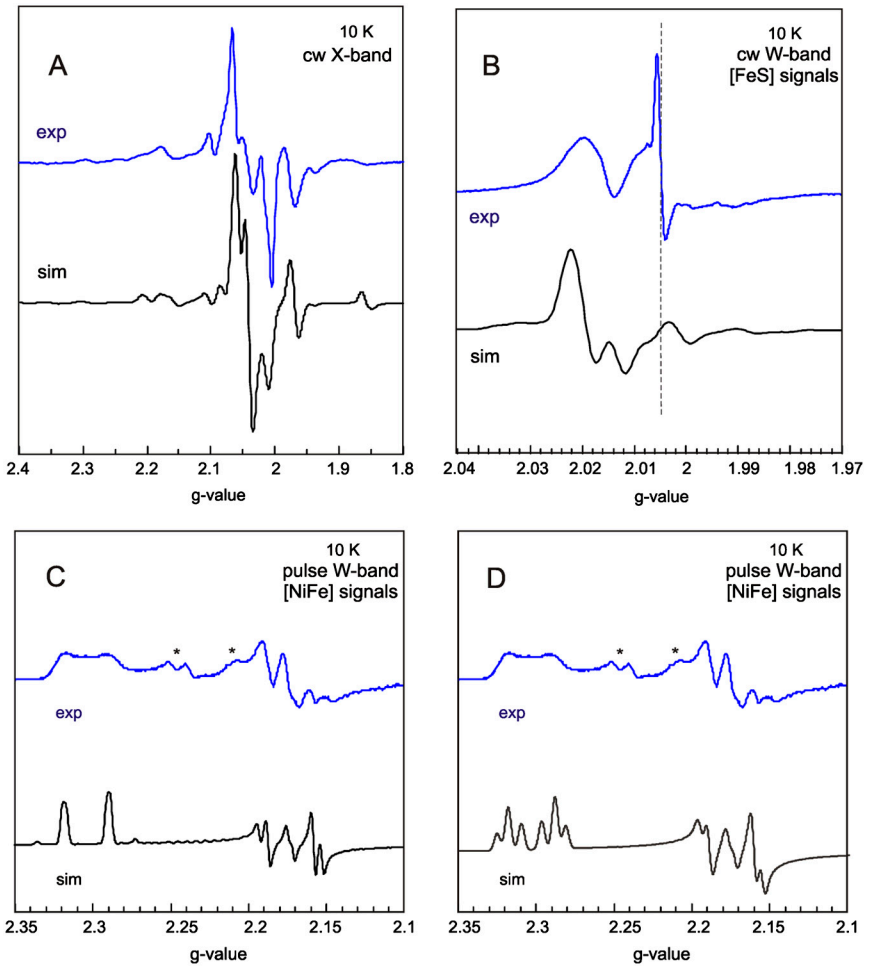

Fig. S8. Spectra (blue traces) of the as-isolated hydrogenase of Hase I from *A. aeolicus* (*A*), at X-band and (*B*, *C*, *D*) at W-band frequency at 10 K. (*B*) shows the iron-sulfur cluster signals and (*C*, *D*) the [NiFe] signals at W-Band. Simulations of the spectra are shown as black traces. The same set of parameters was used to simulate the features of the spectra at these microwave frequencies. The asterisk in (*C*, *D*) marks the signals originating from a state of the molecules that has been termed as Ni-X (unknown) and corresponds to an inactive form of the enzyme (1). Experimental conditions: (cw X-Band) microwave frequency 9.433 GHz, modulation amplitude 1 mT. (pulse W-Band): microwave frequency 94.08 GHz, SRT 0.5 ms, $\pi/2 = 24$ ns, pseudomodulation of (*B*) was performed with 1 mT and of (*C*, *D*) with 3 mT. The dashed line in (*B*) indicates the unreacted porphyrexide radical.

The measurements carried out at W-Band frequency provided (*i*) an upper limit of the isotropic exchange interaction between the [NiFe] site and the proximal HP center, (*ii*) an upper limit for the estimation of the isotropic exchange between the HP center and the [3Fe4S] cluster and (*iii*) an estimation of the principal *g*-values that correspond to the high potential [FeS] center in the proximal to the [NiFe] site position. The simulations approximate the features of the spectra adequately but not perfectly permitting only an estimation of the isotropic *J*-couplings. Due to the large number of unknown parameters (*g*-values of the HP center, relative orientation of the *g*-tensor of the HP center with respect to the [NiFe] site, relative orientation of the g-tensor of the [3Fe4S] cluster with respect to the [NiFe] site, anisotropic dipole-dipole contributions) a unique and exact solution cannot be obtained at present. The principal *g*-tensor of the [NiFe] site used for the simulations was ($g_x = 2.302$, $g_y = 2.172$, and $g_z = 2.013$), for the [3Fe4S] cluster ($g_x = 2.025$ $g_y = 2.018$, and $g_z = 2.010$). The *g*-tensor for the HP center could not be accurately determined. From the simulations the EPR spectrum of the HP center is shown to have small *g*-anisotropy with a $g_{iso} \sim 2$ (i.e., $g_1 = 2.010$, $g_2 = 2.015$, and $g_3 = 1.990$ as used for the simulation shown in *C*). Even small changes in one of the principal *g*-components result in significant changes in the simulations obtained (in *D* the g_1 component was set to $g = 2.020$—relative orientations of the *g*-components were varied for a better fit). At present both solutions are acceptable. Therefore from these experiments we can only estimate the isotropic exchange between the centers and show that the *g*-tensor of the HP center has very small *g*-anisotropy. These conclusions are schematically described in Fig. S9 assuming a topology of the iron-sulfur cofactors similar to that of the oxygen-sensitive hydrogenases, for which high-resolution X-ray structures are available.

1 Pandelia ME, et al. (2010) Membrane-bound hydrogenase I from the hyperthermophilic bacterium *Aquifex aeolicus*: enzyme activation, redox intermediates and oxygen tolerance. *J Am Chem Soc* 132:6991–7004.

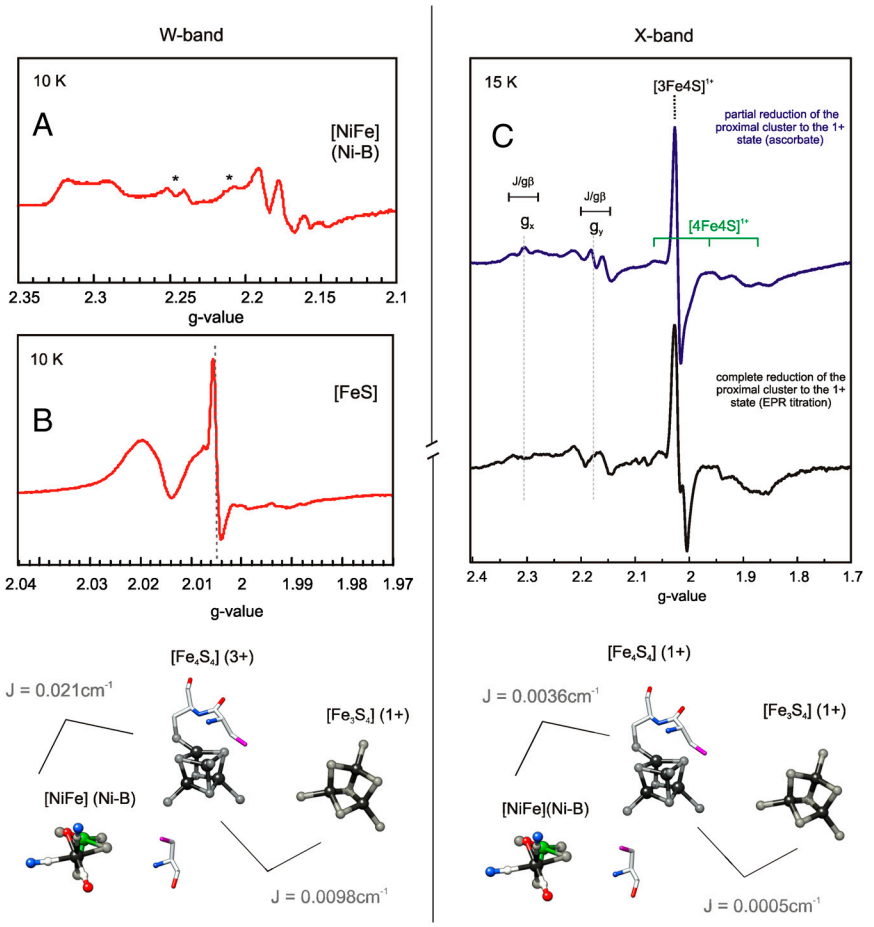

Fig. S9. (Left column) W-band EPR spectrum of the fully oxidized Hase I showing (*A*) the [NiFe] signals and (*B*) the iron-sulfur signals at 10 K. The dashed line in (*B*) indicates the unreacted porphyrexide radical. (Right column) (*C*) X-Band cw EPR spectra obtained under mild reducing conditions achieved both with sodium ascorbate (1 equivalent) and electrochemically (+12 mV). An illustration of the respective coupling schemes are included in each column describing the corresponding interactions between the three ($S = 1/2$) centers. The asterisks in (*A*) denote the presence of a second EPR-active oxidized intermediate that is occasionally present in the samples.

The isotropic exchange coupling between the [NiFe] site in the Ni-B state and the proximal [4Fe4S] cluster that is formally in the 3+ state was estimated by simulating spectra that were recorded using high-field EPR at W-Band (~94 GHz), in which we approach a limit where the exchange interaction becomes much smaller than the Zeeman splitting. There is a significant isotropic exchange (0.021 ± 0.002 cm^{-1}) between the [NiFe] site and the proximal cluster, as well as the proximal cluster and the $[3Fe4S]^{1+}$ center (0.0098 ± 0.0005 cm^{-1}). When the proximal cluster attains its 1+ state (*C*), that is usually found for such systems, the magnitude of the isotropic exchange between the latter and the [NiFe] site in the Ni-B state becomes almost an order of magnitude smaller (0.0036 ± 0.0003 cm^{-1}). Note that 1 cm^{-1} corresponds to 30.000 MHz.

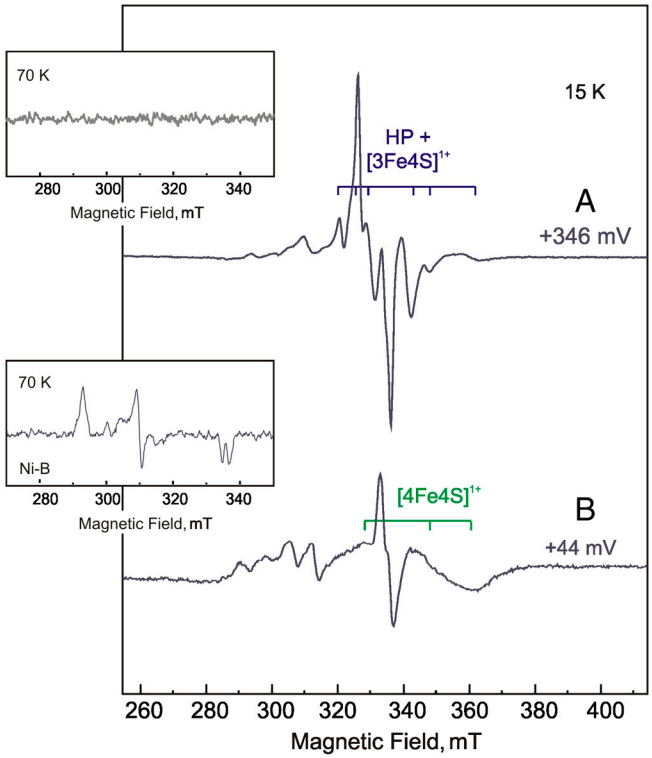

Fig. S10. cw X-Band EPR spectra at pH 6.4 poised at (*A*) +346 mV, (*B*) +44 mV. Experimental conditions: microwave frequency 9.433 GHz, modulation amplitude 1 mT, mw power 2.0 mW, 15 K. The insets show the spectra recorded at $T = 70$ *K* and at 20 mW. At +346 mV and annealing the temperature to 70 K results in the disappearance of the nickel signals showing that the relaxation behavior of the latter has changed. These spectra show that the HP center magnetically interacts both with the $[3Fe4S]^{1+}$ cluster and the nickel-iron site (spin-spin and spin-lattice relaxation enhancement). The peculiar relaxation enhancement of the [NiFe] signals is in agreement with the about one order of magnitude larger isotropic exchange found for the Ni-B and the proximal [4Fe4S] cluster in its superoxidized state (refer to Fig. S9 and to the main text of the manuscript).

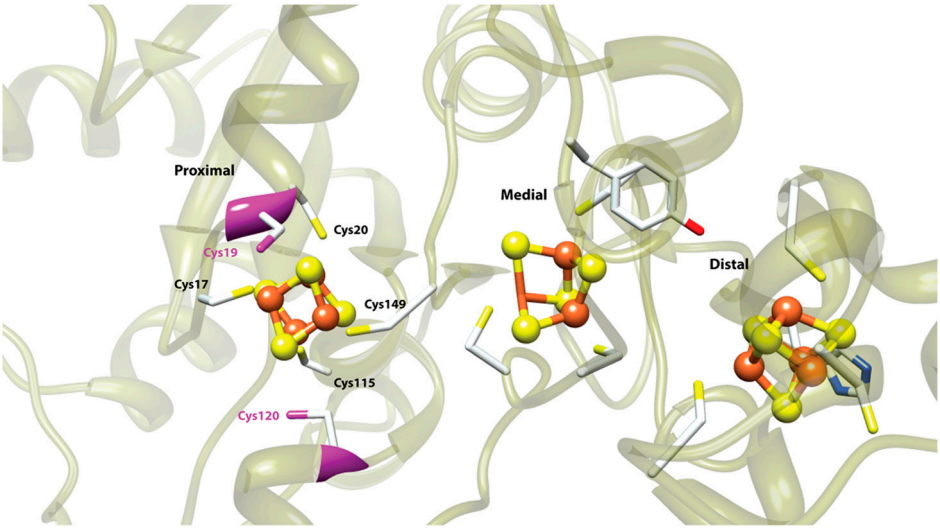

Fig. S11. A "zoomed" view on the homology model of the small subunit of the Hase I from *A. aeolicus* overlaid on the structure of the *D. vulgaris* MF hydrogenase, from which only the metal centers are shown. The extra cysteines can potentially ligate the proximal cluster and thus modulate its redox properties, accounting for its increased capacity to carry out *two* single-electron transitions that are known to not occur in the same center in biological systems. From the Mössbauer data the proximal cluster appears to have a unique Fe subsite that has an unprecedented large quadrupole splitting, compared to those for Fe sites in a tetrahedral coordination environment (i.e., as in the case of the standard hydrogenases). Comparison with model compounds of cubane clusters (1–4) suggests a distorted coordination environment of this Fe, indicating that the cluster is five-coordinated (i.e., the special subsite is suggested from the Mössbauer data to be coordinated by *two-cysteine residues*). The plasticity of the proximal cluster to undergo in a reversible way two single-electron transitions and to reconcile redox couples that were up to date not found to occur within a biological meaningful range is assigned to the additional cysteine ligands that can participate in its coordination, change the overall charge of the cluster core, impose geometrical distortions, affect Fe-S covalencies and hydrogen bonding, and thus may modulate the redox properties of the latter.

1 Kanatzidis MG, Coucouvanis D, Simopoulos A, Kostikas A, Papaefthymiou V (1985) Synthesis, structural characterization, and electronic properties of the tetraphenylphosphonium salts of the mixed terminal ligand cubanes $Fe_4S_4(Et_2Dtc)_n(X)_{4n}^{2-}$ ($X = Cl^-$, PhS^-) ($n = 1, 2$). Two different modes of ligation on the $[Fe_4S_4]^{2+}$ core. *J Am Chem Soc* 107:4925–4935.

2 Kanatzidis MG, Ryan M, Coucouvanis D, Simopoulos A, Kostikas A (1983) Synthesis and structural characterization of Bis(Tetraphenylphosphonium) Bis(Diethyldithiocarbamato)Bis (Thiophenolato)Tetrakis(Mu-3-Sulfido)Tetra Ferrate (2Ii,2Iii), $(Ph_4P)_2[Fe_4S_4(SPh)_2(Et_2dtc)_2]$. A cubane type cluster with mixed terminal ligands and two different modes of ligation on the Fe_4S_4 core. *Inorg Chem* 22:179–181.

3 Ciurli S, et al. (1990) Subsite-differentiated analogs of native $[4Fe\text{-}4S]^{2+}$ clusters—preparation of clusters with 5-coordinate and 6-coordinate subsites and modulation of redox potentials and charge-distributions. *J Am Chem Soc* 112:2654–2664.

4 Johnson RE, Papaefthymiou GC, Frankel RB, Holm RH (1983) Effects of secondary bonding interactions on the $[Fe_4S_4]^{2+}$ core of ferredoxin site analogs—$[Fe_4S_4(Sc_6H_4\text{–}o - OH)_4]^{2-}$, a distorted cubane-type cluster with one five-coordinate iron atom. *J Am Chem Soc* 105:7280–7287.

Table S1. Principal *g*-values of the medial [3Fe4S] cluster in the *A. aeolicus* and *D. vulgaris* MF [NiFe] hydrogenases (1)

Species	g_x	g_y	g_z
D. vulgaris MF	2.0258	2.0174	2.0110
A. aeolicus	2.0256	2.0161	2.0104

1 Brecht M (2001) Hochfeld- und Puls-EPR-Untersuchungen an den Kofaktoren von [NiFe]-Hydrogenasen: Beiträge zur Klärung des Mechanismusses der biologischen Wasserstoffspaltung,Technische Universität Berlin, Doctoral thesis.

Table S2. Apparent midpoint potentials (E_m) for the paramagnetic species in *A. aeolicus* Hase I, at pH 6.4, 7.4 and 8.3, respectively

Species	E_m, mV (pH 6.4)	E_m, mV (pH 7.4)	E_m, mV (pH 8.3)
HP (High Potential)	+232	+232	n.d.
$[3Fe4S]^{1+/0}$	+78	+68	+66
$[4Fe4S]^{2+/1+}$ prox.	+98	+87	+30
$[4Fe4S]^{2+/1+}$ distal	−65	−78	−132
Ni-B split (appear)	+107	+95	+23
Ni-B reduction	−67	−96	−140

The error in the determination of the values is ±20 mV. The appearance of the splitting in the Ni-B titrates with the same midpoint potential as the $[4Fe4S]^{2+/1+}$ couple, showing that reduction of the latter is responsible for the interaction patterns observed in the Ni-B signals

Table S3. Mössbauer parameters for the spectrum of the fully oxidized enzyme (using porphyrexide) from *A. aeolicus* recorded at zero magnetic field and at high-temperature (160 K, fast relaxation limit); isomer shifts (δ), quadrupole splittings (ΔE_Q) and Lorentzian linewidths (Γ).

Species	δ (mms^{-1})	ΔE_Q(mms^{-1})	Γ (mms^{-1})	Formal oxidation state	Sites
[NiFe]	0.12	0.51	0.32	Fe(2+)	1
$[3Fe4S]^{1+}$	0.26	0.60	0.34	Fe(3+)	3
$[4Fe4S]^{2+}$	0.37	0.92	0.36	Fe(2.5+)	3
	0.40	1.23	0.36	Fe(2.5+)	1
$[4Fe4S]^{3+}$	0.46	2.41	0.25	Fe(2.5+)	1
	0.26	0.60	0.34	Fe(3+)	2
	0.40	1.23	0.36	Fe(2.5+)	1

The Mössbauer parameters are identical to the ones of the as-isolated enzyme (Fig. 6 in the main manuscript), but the analysis was carried out first in the fully oxidized enzyme because it is a well defined state (maximized coupled species). Results are consistent with the presence of one three-iron cluster, two four-iron clusters, and a low-spin Fe^{2+} of the [NiFe] active site (12 Fe ions in-total). In the superoxidized state of the enzyme, the iron-sulfur cluster localized proximal to the [NiFe] position is found to formally behave as a HiPIP-like core, having attained a formal oxidation state of 3+. This cluster has a unique Fe subsite with an unusual large magnitude of the electric-field gradient ($\Delta E_Q = 2.41$ mms^{-1}) indicating that it is found in a rather distorted geometry that deviates from the conventional tetrahedral one with an additional coordinating (protein) ligand (1–4)

1 Kanatzidis MG, Coucouvanis D, Simopoulos A, Kostikas A, Papaefthymiou V (1985) Synthesis, structural characterization, and electronic properties of the tetraphenylphosphonium salts of the mixed terminal ligand cubanes $Fe_4S_4(Et_2Dtc)_n(X)_{4n}^{2-}$ ($X = Cl^-$, PhS) ($n = 1, 2$). Two different modes of ligation on the $[Fe_4S_4]^{2+}$ core. *J Am Chem Soc* 107:4925–4935.

2 Kanatzidis MG, Ryan M, Coucouvanis D, Simopoulos A, Kostikas A (1983) Synthesis and structural characterization of Bis(Tetraphenylphosphonium) Bis (Diethyldithiocarbamato)Bis(Thiophenolato)Tetrakis(Mu-3-Sulfido)Tetra Ferrate (2Ii,2Iii), $(Ph_4P)_2[Fe_4S_4(SPh)_2(Et_2dtc)_2]$. A cubane type cluster with mixed terminal ligands and 2 different modes of ligation on the Fe_4S_4 core. *Inorg Chem* 22:179–181.

3 Ciurli S, et al. (1990) Subsite-differentiated analogs of native $[4Fe\text{-}4S]^{2+}$ clusters—preparation of clusters with 5-coordinate and 6-coordinate subsites and modulation of redox potentials and charge distributions. *J Am Chem Soc* 112:2654–2664.

4 Johnson RE, Papaefthymiou GC, Frankel RB, Holm RH (1983) Effects of secondary bonding interactions on the $[Fe_4S_4]^{2+}$ core of ferredoxin site analogs—$[Fe_4S_4(SC_6H_4\text{–o} - OH)_4]^{2-}$, a distorted cubane-type cluster with one five-coordinate iron atom. *J Am Chem Soc* 105:7280–7287.